INVESTIGATION OF THE FUNCTIONAL PROPERTIES OF STRONTIUM HEXAFERRITE $SrFe_{12-x}Cr_xO_{19}$, DOPED WITH CHROMIUM, WITH A DEGREE OF SUBSTITUTION X UP TO 7.5

Alena Zykova[1], Andrey Kovalev[1], Darya Sherstyuk[1], Vladimir Zhivulin[1], Denis Vinnik[1,2,3], Sergey Lezhnev[4], Evgeniy Panin[5], Evgeny Trofimov[1]

[1]*South Ural State University, Chelyabinsk, Russia, zykovaar@susu.ru (A.Z.); kovalev-andrey-i@mail.ru (A.K.); sherstiukd@susu.ru (D.S.); zhivulinve@mail.ru (V.Z.); vinnikda@susu.ru (D.V.); trofimovea@susu.ru (E.T.).*
[2]*Moscow Institute of Physics and Technology Dolgoprudny, Russia, vinnikda@susu.ru (D.V.)*
[3]*St. Petersburg State University, St. Petersburg Russia, vinnikda@susu.ru (D.V.)*
[4]*Rudny Industrial University, Rudny Kazakhstan, sergey_legnev@mail.ru (S.L.)*
[5]*Karaganda Industrial University, Temirtau Kazakhstan, ye.panin@tttu.edu.kz (E.P.)*

Received 29 October 2025
Accepted 04 May 2026
DOI: 10.59957/jctm.v61.i4.2026.16

ABSTRACT

Strontium hexaferrite with a high degree of iron substitution by chromium ($SrFe_{12-x}Cr_xO_{19}$, at x = 6.5 - 7.5 with a step of x(Cr) = 0.5) was obtained by solid - phase synthesis at an isothermal exposure temperature of 1500°C. Analysis of the results of XRD X - ray diffraction and scanning electron microscopy (SEM) confirmed the formation of single - phase hexagonal M - type ferrites upon substitution with Cr ions from x = 6.5 to x = 7.5. Previously, using the same method at a temperature of 1400°C, we synthesized and obtained the results of X - ray, morphology, elemental analyses and magnetic properties for single-phase samples of $SrFe_{12-x}Cr_xO_{19}$ with x = 0 - 6 [1]. This article studies the effect of doping with Cr^{3+} ions on the structural and functional properties of hexaferrite $SrFe_{12-x}Cr_xO_{19}$ x = 0 - 7.5. The temperature and frequency dependences of the initial magnetic permeability of the obtained ferrites have been studied. It was found that the substitution of iron with chromium leads to a decrease in the Curie temperature. Studies of the electrical properties of the obtained materials were carried out in the frequency range of 25 Hz - 3 MHz at room temperature. An analysis of the dielectric properties showed that an increase in the content of Cr^{3+} ions in $SrFe_{12-x}Cr_xO_{19}$ leads to a decrease in the dielectric constant, dielectric losses, the tangent of the dielectric loss angle and an increase in the complex resistance. The results of the study demonstrate the dependence of electrical properties on the frequency of the applied field and the concentration of dopant.

Keywords: strontium hexaferrite, chromium substitution, structure, XRD, SEM, Curie temperature, initial magnetic permeability, dielectric losses, dielectric constants, electrical resistance.

INTRODUCTION

Due to their excellent electrical and magnetic properties, hexaferrites are of great commercial importance and are the subject of interest in fundamental research [2]. Ba, Sr M - type hexaferrites are the most widely used materials for permanent ferrite magnets, which are in high demand due to their low cost and chemical stability.

Magnetically hard materials, such as M - type strontium hexaferrites ($SrFe_{12}O_{19}$), are of great interest in the technology of creating integrated circuits; they are used as permanent magnets due to their exceptional magnetic properties [3 - 6]. The

magnetocrystalline anisotropy, high electrical resistivity, and high saturation magnetization of nanocrystalline substituted strontium hexaferrite are promising for many practical applications, such as the manufacture of permanent magnets, magnetic recording media, various components in microwave devices, electromagnetic properties, electronic components, telecommunications and radio frequency devices [7, 8].

Both the magnetic and electrical properties of hexagonal ferrites largely depend on the synthesis conditions and composition, i.e., the number and type of iron - substituting cations in five different Fe^{3+} crystallographic positions. Several methods for the synthesis of doped Sr - hexaferrite are presented in the literature, such as the traditional solid - phase method, sol - gel, autoignition, hydrothermal, microemulsion and coprecipitation [9 - 14].

The most effective way to improve the magnetic properties of SrM ferrite (including saturation magnetization, field anisotropy, coercive force, and magnetic resonance frequency [15]) is to substitute various ions - Sm^{3+}, Mn^{3+}, Ni^{2+}, Al^{3+}, Co^{2+}, Cr^{3+}, Ti^{3+}, Cu^{2+} and Zn^{2+} as single ions and co-doped variants Mn - Ti, Al - Cr, Co - Ti, Mn - Zn, Co - Zr [16 - 25]. Such materials with high electrical resistivity are the most promising for use in microwave devices [26 - 29].

The substitution of Fe^{3+} ions by Cr^{3+} ions is of great interest in studying the magnetic and dielectric properties of hexaferrite, which are necessary for potential applications in radio and other high - frequency devices. Studies of the dielectric properties of hexaferrites with low degrees of iron substitution by chromium or chromium and aluminium (where single - phase samples were obtained for the compositions $Sr_{1-x}Co_xFe_{12-y}Cr_yO_{19}$ at x = 0 - 0.7 and y = 0 - 0.6, and $SrFe1_{2-x-y}Al_xCr_yO_{19}$, where x = y = 0 - 0.2) are presented by I. Bibi et al. and K. Subrahmanya Sarma et al. [30, 31]. Obtaining hexaferrites with a high degree of iron substitution by other ions is an elusive task due to the difficulty of meeting two conditions: controlled production of a single - phase material with high degrees of substitution and particle size conservation in a single - domain region where maximum coercive force is achieved.

Previously, single - phase strontium hexaferrite $SrFe_{12-x}Cr_xO_{19}$ samples with the maximum degree of substitution by chromium atoms x=6 was obtained by solid - phase synthesis at 1400°C; the results of studying magnetic properties are also presented [1]. At that time, no synthesis technique had been developed that could provide higher degrees of substitution: at x > 6, in addition to the hexaferrite phase at 1400°C, low - intensity peaks related to the α-Cr_2O_3/Fe_2O_3 impurity phases occurred. The second stage of work to increase the maximum degree of chromium substitution was the optimization of the synthesis mode: to obtain single - phase samples of barium hexaferrite $BaFe_{12-x}Cr_xO_{19}$ substituted with chromium, synthesis was carried out at three different temperatures of 1400, 1500 and 1600°C [32]. As a result of the study, optimal conditions for the synthesis of single - phase samples of the composition $BaFe_{12-x}Cr_xO_{19}$ with a degree of substitution x = 5, 6, 7 at 1500°C with an isothermal exposure of 5 h were established [32].

As a result of the implementation of this, the third, stage of research to increase the maximum degree of substitution achieved, as well as the study of the properties of the resulting concentration range of substituted strontium hexaferrite, original, previously unreported in the scientific literature, results with scientific novelty were obtained. In continuation of our study of the possibility of replacing strontium hexaferrite with chromium atoms, in this work single - phase samples of strontium hexaferrite with a high degree of chromium substitution ($SrFe_{12-x}Cr_xO_{19}$ at x = 6.5, 7 and 7.5) were obtained by the solid - phase method, and the effects of Cr^{3+} ion substitution of Fe^{3+} ions on the phase composition and lattice parameters were studied. Also, for the first time, the temperature dependences of the initial magnetic permeability values and the effect of the degree of chromium substitution on changes in the structural and dielectric properties of the entire range of $SrFe_{12-x}Cr_xO_{19}$ samples were studied on the obtained materials (both the compositions obtained for the first time and those whose synthesis description and the results of the study of the structure and magnetic properties were previously presented in [1]).

EXPERIMENTAL

Iron oxide (Fe_2O_3), chromium oxide (Cr_2O_3), and strontium carbonate ($SrCO_3$) with the BDA qualification were used as initial components for solid - phase synthesis. To prepare the charge, the initial components were weighed in stoichiometric ratios and crushed with

simultaneous stirring in an agate mortar. After grinding, the mixture was pressed into tablets with a diameter of 8 mm on a hydraulic laboratory press with a force of 5 t cm^{-2}. The samples on a platinum substrate were sintered at a temperature of 1500°C in a tubular furnace with silicon carbide heaters with an isothermal exposure of 5 h in an atmospheric atmosphere.

X - ray phase analysis was performed on a Rigaku Ultima IV powder diffractometer (Cu Ka radiation, room temperature). X - ray images of the samples were recorded in the angle range 2θ from 15° to 75° at a speed of 2° min^{-1}. Based on the X - ray data, the parameters of the elementary crystal cell were calculated. Structural refinements were carried out in the PDXL software using a full - profile analysis using the Rietveld method. The morphology of the sample surface and elemental chemical analysis were studied using a Jeol JSM 7001F scanning electron microscope (SEM) equipped with an energy dispersive X - ray analyser (EDX).

Differential scanning calorimetry (DSC) was carried out to determine the Curie temperature of the samples. Thermogravimetric analysis and differential scanning calorimetry (TGA/DSC) were done on a simultaneous thermal analyser Netzsch STA 449 F3 Jupiter.

The values of the phase transition temperatures of the second kind (Curie temperature) are determined by constructing the temperature dependence of the inductance of a ferrite core. Rectangular toroidal cores with an outer diameter of 7 mm and an inner diameter of 3 mm were prepared from each sample. The height of the torus was 4 mm. 5 coils of 0.2 mm diameter copper wire were wound around the torus. The inductance L was measured using an E7 - 30 immittance meter at a frequency of 1 MHz. The dielectric properties were studied in the frequency range from 25 Hz to 3 MHz at room temperature on an immittance meter. The disc - shaped surfaces of each sample were coated with silver paste to improve contact with the two electrodes.

RESULTS AND DISCUSSION

Fig. 1 shows X - ray images of single - phase samples recorded in the range of 2 theta angles from 15 to 75° with a shooting speed of 2° min^{-1}. The literature data for unsubstituted strontium hexaferrite $SrFe_{12}O_{19}$ are represented by a bar chart [33]. X - ray phase analysis showed that the formation of single - phase chromium - substituted strontium hexaferrite at a synthesis temperature of 1500 °C is possible up to 7.5. The identified phase is isostructured to a magnetoplumbite

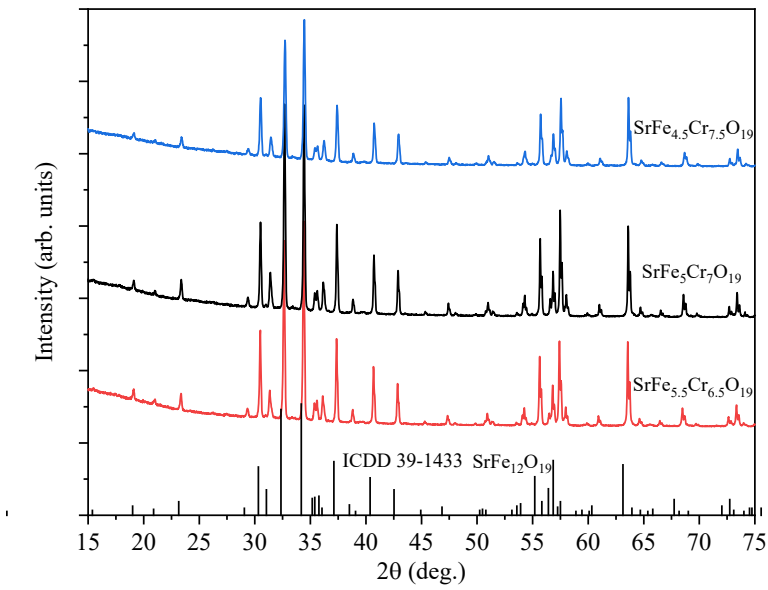

Fig. 1. Diffractograms of the $SrFe_{12-x}Cr_xO_{19}$ system (at x from 6.5 to 7.5) synthesized at 1500°C.

with the space group P63/mmc. At x = 8.0, impurity phases (α-Cr_2O_3/Fe_2O_3 were detected, and intermediate reaction products, $SrCr_2O_4$ and Fe_3O_4, were identified. Thus, it was possible to obtain single - phase $SrFe_{12-x}Cr_xO_{19}$ samples with a maximum degree of substitution x up to 7.5 at a temperature of 1500°C.

Based on the results of X - ray phase analysis using the Rietveld method, the unit cell parameters were calculated in the PDXL software package. Table 1 contains these data, as well as refinement parameters and coherent scattering region size (D), which is proportional to particle size. Refinement parameter values are lower than 10 %, so experimental XRD patterns are in good agreement with simulated theoretical pattern. With $x = 7$, size of coherent scattering regions is about 50 % higher than with x = 6.5 or 7.5.

The substitution of iron with chromium led to a decrease in the parameters of the crystal lattice a, c, and volume V. This can be explained by the difference in the values of the ion radius of iron and chromium: $r(Fe^{3+})$ $CN^{VI} = 0.645$ Å; $r(Cr^{3+})$ $CN^{VI} = 0.615$ Å [34]. This result correlates with previously obtained values and literature data [1, 32, 35].

The data of the elemental analysis and the calculated actual formulas of the samples are presented in the Table 2. In general, the coefficients of the calculated gross formulas calculated according to the results of the energy - dispersion analysis correlate with the values of the initial calculated gross formulas.

Electron microscopic examination allowed us to establish that the obtained samples should be characterized by a uniform distribution of elements in their structure. The morphology of the surface of the samples consists of a multitude of differently oriented hexagonal particles soldered together. Fig. 2 shows SEM images of the obtained samples.

The study of the temperature dependence of the real and imaginary parts of the magnetic permeability for the entire range of synthesized $SrFe_{12-x}Cr_xO_{19}$ samples (x up to 7.5) was carried out in the temperature range of 50 - 600°C. The temperature dependences of the imaginary and real parts of the initial magnetic permeability of

Table 1. Unit cell parameters of the obtained solid solutions.

Sample formula	*a*, Å	*c*, Å	*c/a*	*V*, Å^3	R_{wp}, %	R_{exp}, %	χ^2	D, nm
$SrFe_{5,5}Cr_{6,5}O_{19}$	5.8412(5)	22.741(5)	3.8932	671.950(11)	6.9	3.1	5.0	41.5
$SrFe_5Cr_7O_{19}$	5.8410(4)	22.7226(14)	3.8902	671.380(7)	8.4	2.9	8.2	61.8
$SrFe_{4,5}Cr_{7,5}O_{19}$	5.8367(4)	22.6872(15)	3.8870	669.340(7)	7.6	2.8	7.2	42.4

Table 2. The results of the elemental analysis and calculated gross formulas of the samples.

Sample	Elemental composition, at. %			Actual formula
	Sr	Fe	Cr	
$SrFe_{5,5}Cr_{6,5}O_{19}$	1.00	5.51	6.49	$SrFe_{5.51}Cr_{6.49}O_{19}$
$SrFe_5Cr_7O_{19}$	1.00	4.63	7.37	$SrFe_{4.63}Cr_{7.37}O_{19}$
$SrFe_{4,5}Cr_{7,5}O_{19}$	1.00	4.23	7.77	$SrFe_{4.23}Cr_{7.77}O_{19}$

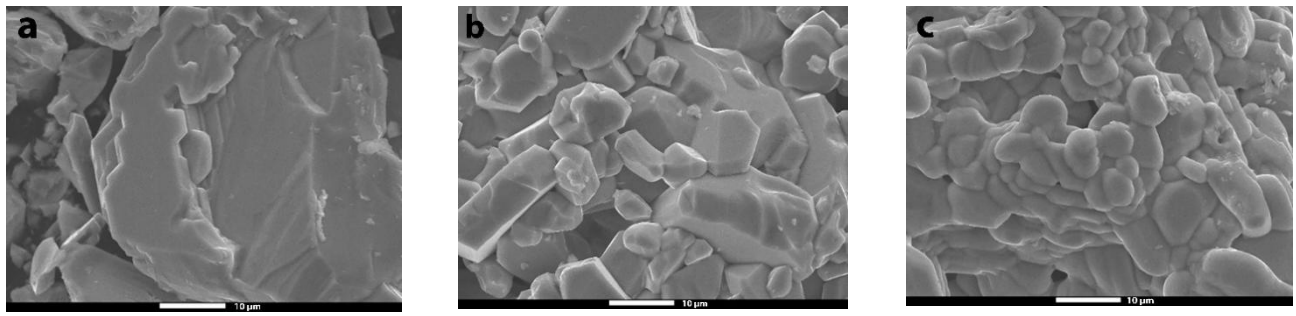

Fig. 2. SEM images of samples: (a) $SrFe_{5.5}Cr_{6.5}O_{19}$, (b) $SrFe_5Cr_7O_{19}$, (c) $SrFe_{4.5}Cr_{7.5}O_{19}$.

the samples (at x up to 5) are shown in Fig. 3. For samples with degrees of substitution greater than 5, it was impossible to determine the temperatures of the beginning and end of the paramagnetic transition.

As can be seen, the temperature dependences of the real part of the magnetic permeability for samples with different degrees of substitution have a different appearance. All the studied samples near the temperature

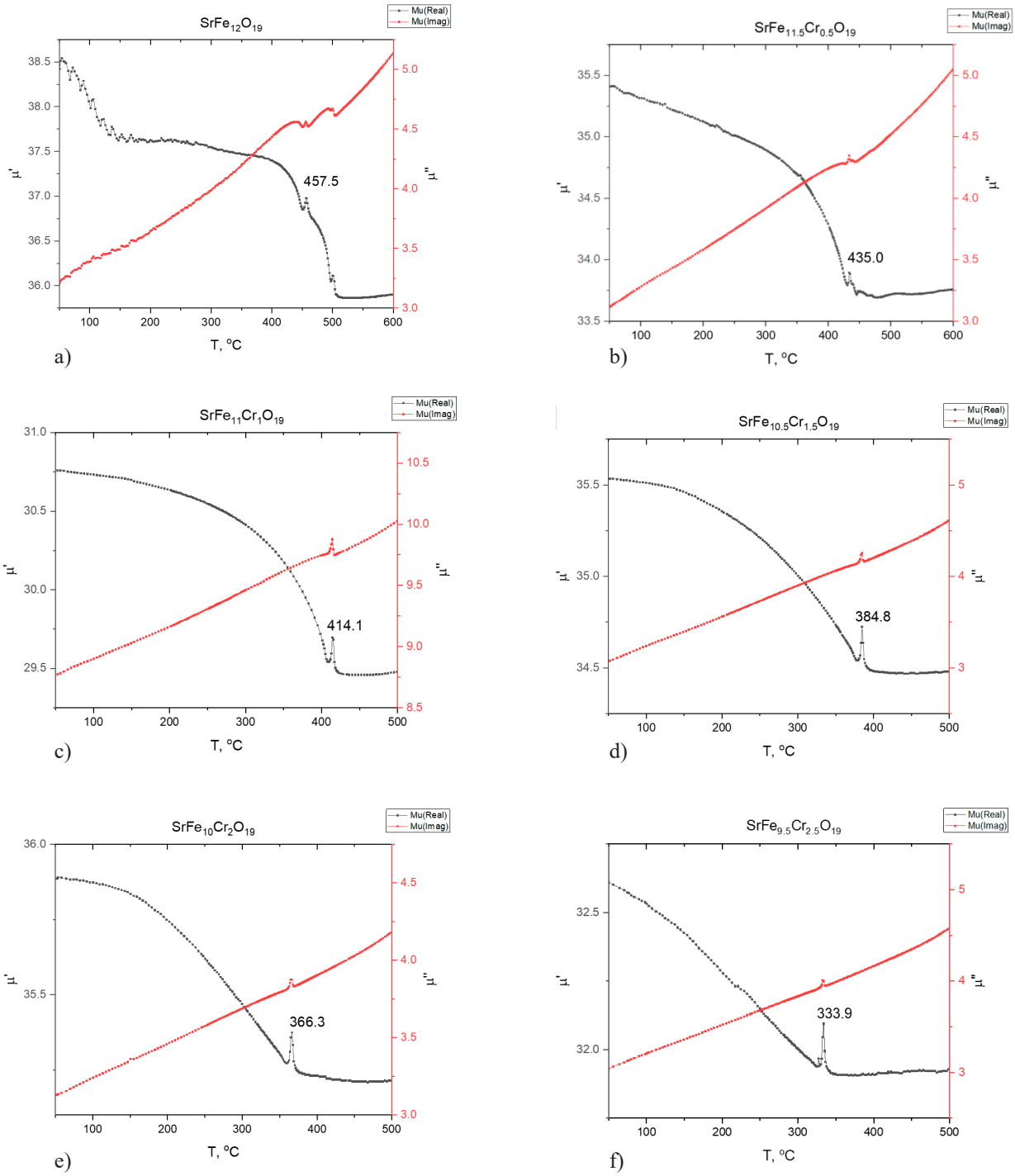

Fig. 3. Dependences of the magnetic permeability with the marked Curie temperature for $SrCr_xFe_{(12-x)}O_{19}$ samples. The black line indicates the data for the real part of the initial magnetic permeability (μ'). The red line indicates the data for the imaginary part of the initial magnetic permeability (μ').

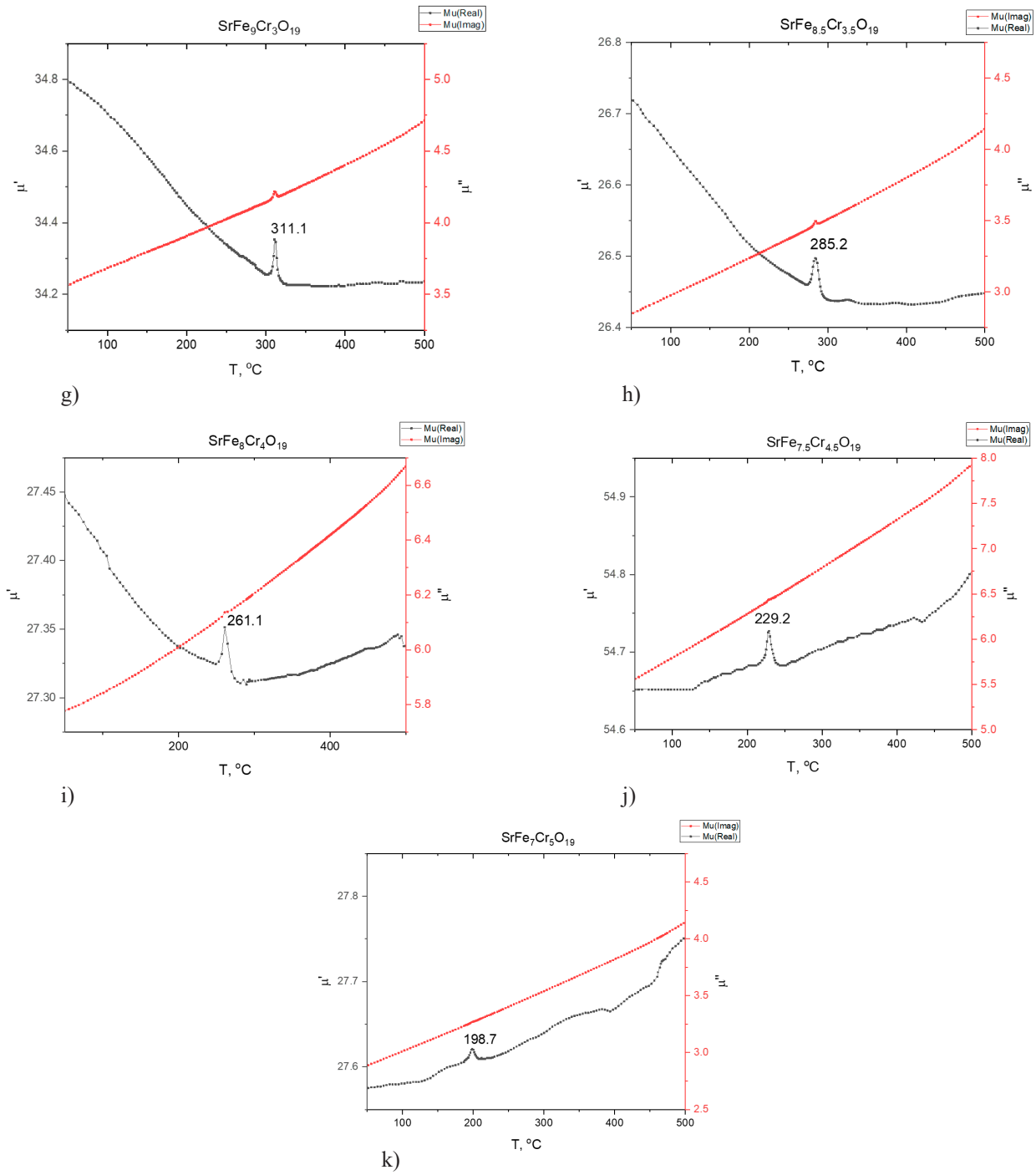

Fig. 3. Dependences of the magnetic permeability with the marked Curie temperature for $SrCr_xFe_{(12-x)}O_{19}$ samples. The black line indicates the data for the real part of the initial magnetic permeability (μ'). The red line indicates the data for the imaginary part of the initial magnetic permeability (μ').

of the magnetic phase transition have a narrow low - intensity peak. The temperature of the end and beginning of the magnetic phase transition, as well as the peak temperature, decreases with increasing degree of chromium substitution (Table 3). The temperature dependence of the imaginary part of the magnetic permeability for all studied $SrFe_{12-x}Cr_xO_{19}$ samples increases with increasing measurement temperature.

The obtained dependences can be interpreted as the approximation of ferrimagnets to the paramagnetic

Table 3. The temperature of the beginning and end of the magnetic phase transition, as well as the peak temperature of the obtained samples.

Sample formula	T (start), °C	T (peak), °C	T (end), °C
$SrFe_{12}O_{19}$	432.6	457.5	495.4
$SrFe_{11,5}Cr_{0,5}O_{19}$	387.1	435	433.2
$SrFe_{11}Cr_{1}O_{19}$	359	414.1	415.1
$SrFe_{10,5}Cr_{1,5}O_{19}$	248.2	384.8	388.7
$SrFe_{10}Cr_{2}O_{19}$	184.5	366.3	369.5
$SrFe_{9,5}Cr_{2,5}O_{19}$	131.5	333.9	336.3
$SrFe_{9}Cr_{3}O_{19}$	113.3	311.1	313.7
$SrFe_{8,5}Cr_{3,5}O_{19}$		285.2	298.0
$SrFe_{8}Cr_{4}O_{19}$		261.1	270.7
$SrFe_{7,5}Cr_{4,5}O_{19}$		229.2	
$SrFe_{7}Cr_{5}O_{19}$		198.7	

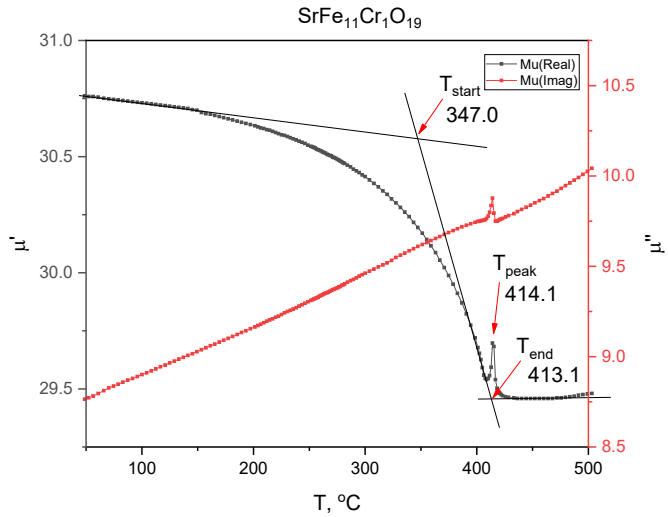

Fig. 4. Graph of the temperature dependence of the real part of the magnetic permeability (black dots) and the imaginary part (red dots) of the $SrFe_{11}CrO_{19}$ sample.

transition temperature (Curie temperature) from the low temperature range, when the magnetic permeability decreases. Such a transition was characterized by the temperature values of the start of the process, the end of the process and the point of extremum. The temperatures of the beginning and end of the paramagnetic transition are determined by the tangent method. Fig. 4 shows the temperature dependence of the initial magnetic permeability of the $SrFe_{11}CrO_{19}$ sample.

Hexaferrites with relatively low degrees of substitution are characterized by a decrease in the real part of the magnetic permeability with increasing temperature. However, starting from the degree of chromium 4.5 substitution, the reverse situation is observed, when the real component begins to increase. The temperature of the beginning of the transition can be determined by the tangent method at degrees of substitution 0 - 3, whereas further it becomes impossible. It is assumed that with an increase in the degree of substitution, both the beginning and the end of the process shift towards low temperatures, which is why, already at the degree of substitution 3.5, the beginning of the process goes beyond the temperature range under study. In addition, as the degree of substitution increased,

as already noted, the nature of the dependence of the real part of the magnetic permeability changed. As a result, after the degree of substitution of 4, it is impossible to determine the end temperature of the process using the tangent method. The values obtained by the described method correlate with the Curie temperature values determined by differential scanning calorimetry (Fig. 5).

It was found that the substitution of iron with chromium leads to a decrease in the Curie temperature. The $SrFe_6Cr_6O_{19}$ - $SrFe_{4.5}Cr_{7.5}O_{19}$ samples are no longer ferrimagnetic, so the Curie temperatures do not matter. The value of the transition point from the ferrimagnetic to the paramagnetic state is determined by the strength of the super - exchange interaction between the cations. Ion substitution, changes in bond length and angles between metal cations and anions, as well as the inclusion of non - magnetic or less magnetic cations in the composition can cause a decrease in the super - exchange interaction. In this case, as the degree of chromium substitution increases, the number of Cr^{3+} - O^{2-} bonds increases due to a decrease in the number of Fe^{3+} - O^{2-} bonds. This leads to a decrease in the interaction, since the magnetic moment of Cr^{3+} is less than that of the substituted Fe^{3+}.

The results obtained in the framework of the study make it possible to expand the understanding of the properties, particularly the Curie temperature, of $SrFe_{12-x}Cr_xO_{19}$ materials in a wide range of degrees of substitution. The resulting range of materials has the potential to be used as materials for self - calibrating temperature sensors with an optimized operating temperature range for a specific industry. The values of the dielectric constant of ferrites depend on the types of charge carriers, the synthesis method, the stoichiometry of the chemical composition, the grain size and the temperature regime of heating. Change in dielectric constant as a function of frequency for $SrFe_{12-x}Cr_xO_{19}$ hexaferrite samples (x up to 7.5) at room temperature is shown in Fig. 6.

At low frequencies, a higher value of the dielectric constant is observed, which may be related to the mechanisms described in [36]. If the nature of the interaction of charge carriers in the grain boundary is abrupt, then due to the high charge concentration at the interfaces, an increase in interphase polarization can be observed in the system. In this case, the value of the dielectric constant increases. With an increase in the frequency of radiation, charge carriers can change their trajectory, which means that the probability of approaching the grain boundary will decrease, and the contribution to the overall polarization will increase, which ultimately leads to a decrease in the dielectric constant [37].

The values of the dielectric constant of the $SrFe_{12-x}Cr_xO_{19}$ samples decrease with an increase in the content of Cr^{3+} ions. This may be due to a decrease in the concentration of delocalized carriers during heterovalent substitution. Such a pattern was observed for samples of strontium hexaferrite substituted with neodymium. The authors of the article suggest that the inclusion of Nd^{3+} for Fe^{3+} ions reduces the number of iron ions in octahedral positions, which are responsible for dielectric polarization and prevents the displacement of spatial charge carriers in the direction of the electric field [38].

Fig. 7 shows the frequency dependences of dielectric losses. According to the figure, an increase in frequency leads to a decrease in dielectric losses for all samples. This behaviour of dielectric losses in ferrites is based on the Maxwell - Wagner model and the Koop theory [39 - 42]. It should be noted that an increase in the degree of iron substitution with chromium in the $SrFe_{(12-x)}Cr_xO_{19}$ samples also leads to a dramatic reduction in dielectric

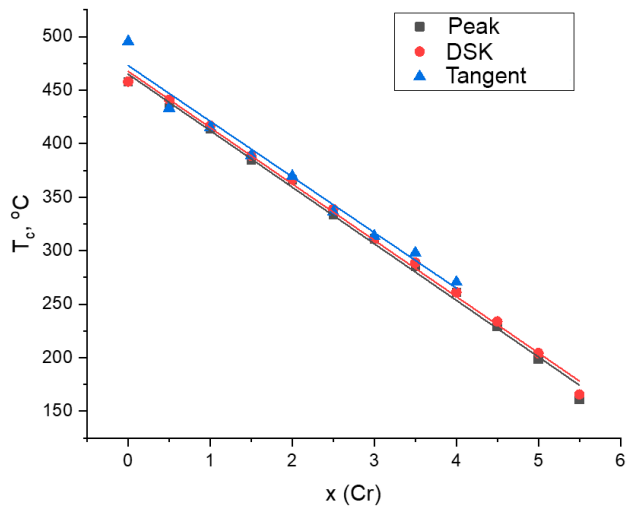

Fig. 5. Dependence of T_C values (determined in different ways) on the degree of chromium substitution of $SrFe_{12-x}Cr_xO_{19}$ samples.

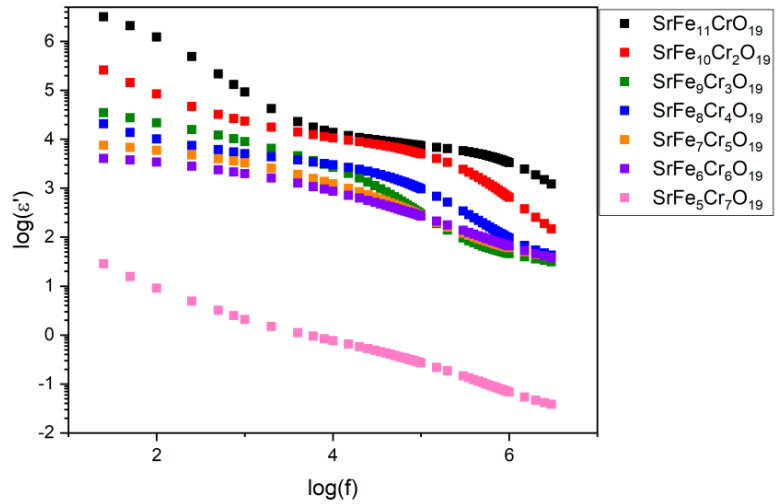

Fig. 6. Frequency dependence of the dielectric constant of $SrFe_{12-x}Cr_xO_{19}$ samples.

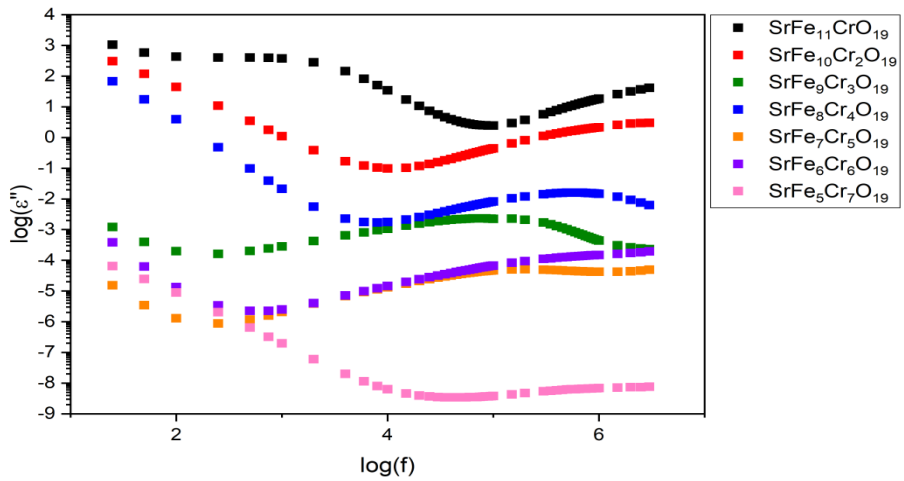

Fig. 7. Frequency dependence of dielectric losses of $SrFe_{12-x}Cr_xO_{19}$ samples.

losses. It is known that the average particle size affects the electrical characteristics of oxide ceramics. This effect is due to a combination of internal factors, such as changes in the parameters of the crystal structure, and external factors, including the presence of defects, residual stresses at the interfaces, porosity, and grain boundaries [43].

Dielectric losses are characterized by the values of the tangent of the dielectric loss angle tanδ [44]. The tangent of dielectric losses also depends on the structure, which depends on the sintering temperature of the samples [45]. Change in the tangent of the dielectric loss angle as a function of frequency for $SrFe_{(12-x)}Cr_xO_{19}$ hexaferrite samples is shown in Fig. 8. The Fig. 8 shows that as the degree of substitution increases, tan δ decreases significantly across the entire frequency range, which is critical for high - frequency applications. Low - loss materials can be used in attenuator designs. Figs. 9 and 10 show the resistance measurement for the obtained samples at room temperature.

At low applied frequencies, a higher Z value indicates that polarization occurs rapidly at these frequencies.

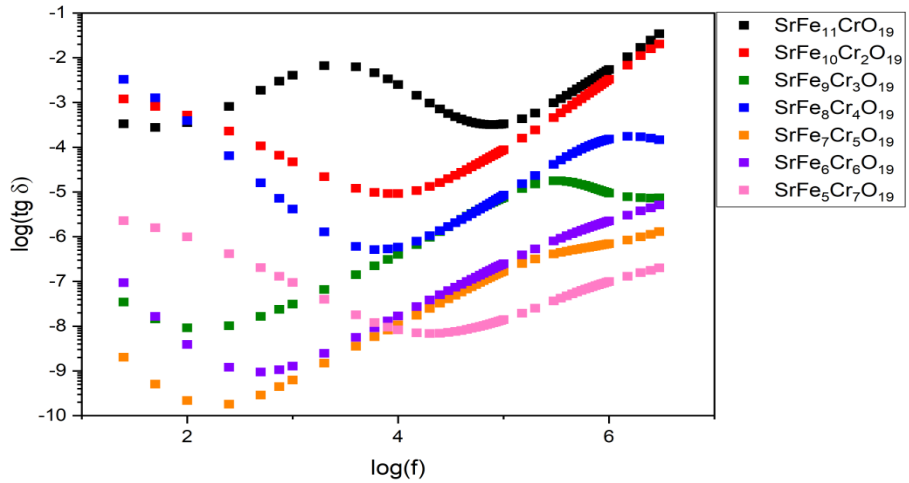

Fig. 8. Frequency dependence of the angle tangent of dielectric loss of $SrFe_{12-x}Cr_xO_{19}$ samples.

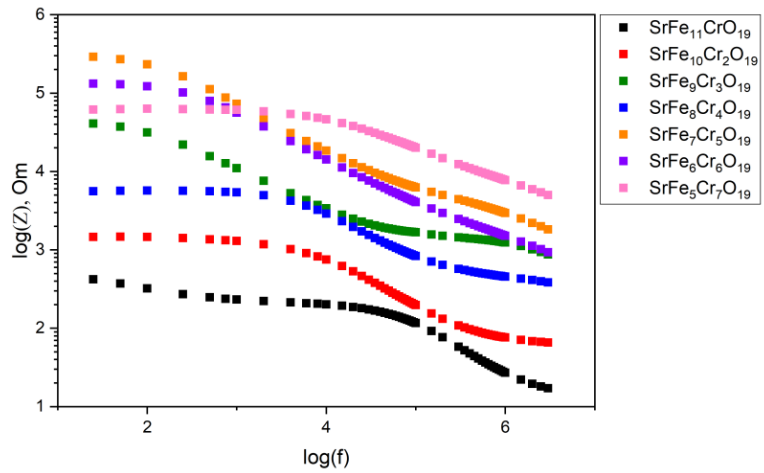

Fig. 9. Frequency dependence of the complex resistance of $SrCr_xFe_{12-x}O_{19}$ samples.

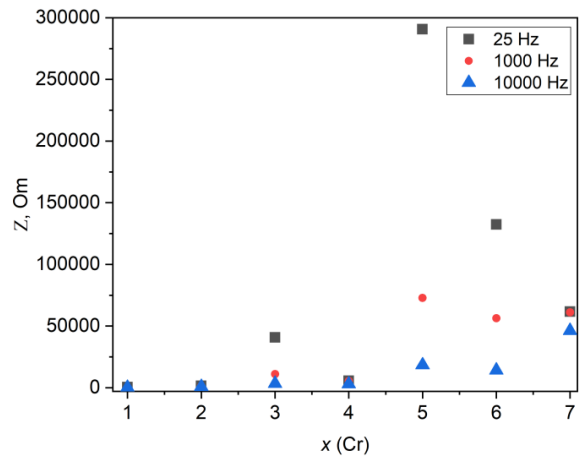

Fig. 10. Frequency dependence of the electrical resistance of $SrFe_{12-x}Cr_xO_{19}$ samples at 25, 1000, 10000 Hz.

Release of space charge polarization at the boundaries with the applied field can occur at higher frequencies. This polarization occurs due to the rapid change in space charge in a stronger applied field. The analysis of the dielectric properties $SrCr_xFe_{(12-x)}O_{19}$ hexaferrite with a high degree of substitution by Cr^{3+} ions and various frequencies provides valuable information for studying the behaviour of charge carriers and polarization mechanisms.

CONCLUSIONS

Strontium hexaferrite with a high degree of chromium substitution x(Cr) = 6.5 - 7.5 was successfully synthesized by solid - phase synthesis. To obtain monophase samples (with space group 194, P6 3/mmc), the synthesis temperature regime was determined at 1500°C with an isothermal exposure of 5 h.

An increase in the degree of chromium substitution from 6.5 to 7.5 leads to a decrease in the unit cell parameters from 5.8412(4) Å to 5.8367(4) Å, parameter a, and from 22.741(5) Å to 22.6872(15) Å, parameter C. A linear decrease in the parameters indicates the production of a continuous series of solid solutions in a given concentration range and successful substitution of Fe^{3+} atoms with Cr^{3+} atoms. The influence of the degree of chromium substitution on the course of the temperature dependence of the initial magnetic permeability is investigated. An increase in chromium concentration leads to a monotonous decrease in the Curie temperature. Based on the type of curves and the presence of a peak in the temperature dependences of the real part of the magnetic permeability for samples with high degrees of chromium substitution, the transition of the material from the ferrimagnetic state to the antiferromagnetic state is assumed. Thus, obtaining monophase samples with a high degree of chromium substitution of a given composition and studying the properties of several materials with a continuous range of Curie temperatures opens up the possibility of their further application in various branches of modern technology. The correlation of the dielectric characteristics of hexaferrite samples with their chemical composition has been established, primarily due to the weakening of bonds between magnetically active Fe^{3+} ions in the ferrite structure and changes in dielectric losses. With an increase in the degree of iron substitution with chromium, a decrease in dielectric constant, dielectric and tangent of the dielectric loss angle, as well as an increase in electrical resistance, was observed.

The results obtained contribute to the understanding of ferrite materials and have potential for possible applications in the field of electronic and telecommunication technologies.

Acknowledgements

The research was carried out at the expense of a grant from the Russian Science Foundation No. 24-29-20187 (https://rscf.ru/project/24-29-20187/).

Authors' contributions

A. Z.: nvestigation, funding acquisition, project administration; A. K.: methodology, investigation, writing - original draft; E. T.: conceptualization, methodology, investigation; D. Sh.: visualization, investigation; V. Z.: validation, data curation; S. L.: software; D. V. : writing - review & editing; E. P. formal analysis, resources.

REFERENCES

1. A.R. Zykova, A.I. Kovalev, D.P. Sherstyuk, V.E. Zhivulin, D.A. Vinnik, S.V. Taskaev, Cr - substituted M - type hexaferrite solid solutions with high level of substitution, Fine Chem. Technol., 2025, 20, 344-356. https://doi.org/10.32362/2410-6593-2025-20-4-344-356.
2. S.E. Rowley, T. Vojta, A.T. Jones, E. Baggio Saitovitch, W. Guo, J. Oliveira, B.E. Watts, F.D. Morrison, J.F. Scott, N. Lindfield, Quantum percolation phase transition and magnetoelectric dipole glass in hexagonal ferrites, Physical Review B, 2017, 96, 020407. https://doi.org/10.1103/PhysRevB.96.020407.
3. Y. Slimani, A. Baykal, A. Manikandan, Effect of Cr^{3+} substitution on AC susceptibility of Ba hexaferrite nanoparticles, J. Magn. Magn Mater., 2018, 458, 204-212. https://doi.org/10.1016/J.JMMM.2018.03.025.
4. M.A. Almessiere, Y. Slimani, H. Gungunes, A. Manikandan, A. Baykal, Investigation of the effects of Tm^{3+} on the structural, microstructural, optical, and magnetic properties of Sr hexaferrites, Results

Phys., 2019, 13, 102166. https://doi.org/10.1016/j.rinp.2019.102166.

5. M. Almessiere, Y. Slimani, N. Algarou, M. Gondal, Y. Wudil, M. Younas, I. Auwal, A. Baykal, A. Manikandan, T. Zubar, Electronic, magnetic, and microwave properties of hard/soft nanocomposites based on hexaferrite $SrNi_{0.02}Zr_{0.02}Fe_{11.96}O_{19}$ with variable spinel phase MFe_2O_4 (M= Mn, Co, Cu, and Zn), Ceram. Int., 2021, 47, 35209-35223. https://doi.org/10.1016/j.ceramint.2021.09.064.
6. M. Almessiere, Y. Slimani, H. Gungunes, M. Nawaz, F. Al-ahmari, A. Manikandan, A. Baykal, Investigation of the crystal/magnetic structure, magnetic and optical properties of $SrY_xNb_xFe_{12-2x}O_{19}$ ($x \leq 0.05$) hexaferrite, Phys. Scripta, 2020, 95, 055802. https://doi.org/10.1088/1402-4896/ab7143.
7. P.A. Lyla, Structural and magnetic properties of spinel Mg-Ni ferrites nanoparticles synthesized by microwave combustion method, Turk. J. Comput. Math. Educ. (TURCOMAT), 2021, 12, 1455-1461.
8. O. Ozturk, A. Nefrow, F. Bulut, S. Kurnaz, S. Safran, Comparison of the dopant effect and sample preparation method on Y-123 superconductors, J. Supercond. Nov. Magn., 2021, 34, 2821-2832, https://doi.org/10.1007/s10948-021-06046-y.
9. M. Sivakumar, A. Gedanken, W. Zhong, Y.W. Du, D. Bhattacharya, Y. Yeshurun, I. Felner, Nanophase formation of strontium hexaferrite fine powder by the sonochemical method using $Fe(CO)_5$, J. Magn. Magn Mater., 2004, 268, 95-104. https://doi.org/10.1016/S0304-8853(03)00479-7.
10. M.A. Almessiere, Y. Slimani, A. Baykal, Structural and magnetic properties of Ce-doped strontium hexaferrite, Ceram. Int., 2018, 44, 9000-9008. https://doi.org/10.1016/j.ceramint.2018.02.101.
11. T.M.H. Dang, V.D. Trinh, D.H. Bui, M.H. Phan, D.C. Huynh, Sol - gel hydrothermal synthesis of strontium hexaferrite nanoparticles and the relation between their crystal structure and high coercivity properties, Adv. Nat. Sci. Nanosci. Nanotechnol., 2012, 3, 025015. https://doi.org/10.1088/2043-6262/3/2/025015.
12. A. Davoodi, B. Hashemi, Investigation of the effective parameters on the synthesis of strontium hexaferrite nanoparticles by chemical coprecipitation method, J. Alloys Compd., 2012, 512, 179-184. https://doi.org/10.1016/j.jallcom.2011.09.059.
13. A. Drmota, M. Drofenik, A. Znidarsic, Synthesis and characterization of nanocrystalline strontium hexaferrite using the co-precipitation and microemulsion methods with nitrate precursors, Ceram. Int., 2012, 38, 973-979. https://doi.org/10.1016/j.ceramint.2011.08.018.
14. I. Bibi, Z. Nazeer, F. Majid, S. Ata, O. Hakami, I. Talib, M. Iqbal, M. Fatima, N. Alfryyan, N. Alwadai, Structural, electrochemical and photocatalytic properties of zinc doped $Co_{1-x}Zn_{1.5x}FeO_3$ perovskites prepared by auto combustion sol-gel approach, Results Phys., 2021, 26, 104392. https://doi.org/10.1016/j.rinp.2021.104392.
15. S. Asiri, S. Güner, A. Demir, A. Yildiz, A. Manikandan, A. Baykal, Synthesis and magnetic characterization of Cu substituted barium hexaferrites, J. Inorg. Organomet. Polym. Mater., 2018, 28, 1065-1071. https://doi.org/10.1007/s10904-017-0735-1.
16. M. Almessiere, Y. Slimani, H. El Sayed, A. Baykal, Ca^{2+} and Mg^{2+} incorporated barium hexaferrites: structural and magnetic properties, J. Sol. Gel Sci. Technol., 2018, 88, 628-638. https://doi.org/10.1007/s10971-018-4853-1.
17. A. Arora, S. B. Narang, K. Pubby, Effect of thickness on microwave absorptive behavior of La-Na doped CoZr barium hexaferrites in 18.0-26.5 GHz band, J. Magn. and Magn. Mater., 2017, 423, 441-446. https://doi.org/10.1016/j.jmmm.2016.09.126.
18. S.M.E. Sayed, T.M. Meaz, M.A. Amer, H.A.E. Shersaby, Magnetic behavior and dielectric properties of aluminum substituted M-type barium hexaferrite, Phys. B: Conden. Mat., 2013, 426, 137-143. https://doi.org/10.1016/j.physb.2013.06.026.
19. S.V. Trukhanov, A.V. Trukhanov, V.O. Turchenko, V.G. Kostishin, L.V. Panina, I.S. Kazakevich, A.M. Balagurov, Magnetic Ordering in $BaFe_{11.9}In_{0.1}O_{19}$ Hexaferrite, J. Low Temp. Phys., 2017, 186, 44-62. https://doi.org/10.1007/s10909-016-1646-1.
20. V.Yu. Ivanov, A.M. Balbashov, A.A. Mukhin, L.D. Iskhakova, M.E. Voronchikhina, Magnetic and magnetoelectric properties of substituted M-type $SrSc_xFe_{12-x}O_{19}$ hexaferrites, J. Exp. Theor. Phys., 2017, 124, 604-611. https://doi.org/10.1134/S10637761170300205.
21. C. Singh, S.B. Narang, M. Jaroszewski,V. Bhikan, P. Kaur, Schottky-Richardson, Poole-Frenkel, and

space charge limited current mechanisms in M-type $Sr(MnTi)_xFe_{(12-2x)}O_{19}$ ferrite, J. Am. Ceram. Soc., 2016, 99, 3639-3644. https://doi.org/10.1111/jace.14390.

22. R.C. Alange, P.P. Khirade, S.D. Birajdar, A.V. Humbe, K.M. Jadhav, Structural, magnetic and dielectrical properties of Al-Cr Co-substituted M-type barium hexaferrite nanoparticles, J. Mol. Struct., 2016, 1106, 460-467. https://doi.org/10.1016/j.molstruc.2015.11.004.
23. S.B. Narang, K. Pubby, C. Singh, Thickness and composition tailoring of K and Ka band microwave absorption of $BaCo_xTi_xFe_{(12-2x)}O_{19}$ ferrites, J. Electron. Mater., 2017, 46, 718-728. https://doi.org/10.1007/s11664-016-5059-3.
24. A. Baykal, M. Demir, B. Unal, H. Sozeri, M.S. Toprak, Synthesis characterization and dielectric properties of $BaFe_{10}(Mn^{2+}Zn^{2+}Zn^{2+})O^{19}$ hexaferrite, J. Supercond. Nov Magn., 2016, 29, 199-205. https://doi.org/10.1007/s10948-015-3232-1.
25. P. Kaur, S.K. Chawla, S.S. Meena, S.M. Yusuf, S.B. Narang, Synthesis of Co-Zr doped nanocrystalline strontium hexaferrites by sol-gel auto-combustion route using sucrose as fuel and study of their structural, magnetic and electrical properties, Ceram. Int., 2016, 42, 14475-14489. https://doi.org/10.1016/j.ceramint.2016.06.053.
26. Y. Slimani, A. Baykal, M. Amir, N. Tashkandi, H. Güngünes, S. Guner, H. El Sayed, F. Aldakheel, T.A. Saleh, A. Manikandan, Substitution effect of Cr^{3+} on hyperfine interactions, magnetic and optical properties of Sr-hexaferrites, Ceram. Int., 2018, 44, 15995-16004. https://doi.org/10.1016/j.ceramint.2018.06.033.
27. M. Almessiere, Y. Slimani, A.D. Korkmaz, S. Güner, A. Maarouf, A. Baykal, Comparative study of sonochemically synthesized Co-Zr and Ni-Zr substituted Sr hexaferrites: magnetic and structural investigations, J. Magn. Magn Mater., 2020, 497, 165996. https://doi.org/10.1016/j.jmmm.2019.165996.
28. T. Phan, H. Nguyen, W. Jeong, R. Idczak, V. Tran, D. Yang, B. Lee, X-ray absorption and Mossbauer spectra, and microwave absorption of (Co, Mn)-doped $SrFe_{12}O_{19}$ hexaferrites, Curr. Appl. Phys., 2021, 29, 114-121. https://doi.org/10.1016/j.cap.2021.07.002.
29. A. Thakur, R. Singh, P. Barman, Synthesis and characterizations of Nd^{3+} doped $SrFe_{12}O_{19}$ nanoparticles, Mater. Chem. Phys., 2013, 141, 562-569. https://doi.org/10.1016/j.matchemphys.2013.05.063.
30. I. Bibi, S. Iqbal, F. Majid, N. Fatima, N. Alwadai, M. Iqbal, Solar-light-driven photocatalytic performance of Cr and Co doped $Sr_{1-x}Co_xFe_{12-y}Cr_yO_{19}$ and effect of doping on optical, structural and dielectric properties, Opt. Mat., 2022, 124, 111961. https://doi.org/10.1016/j.optmat.2021.111961.
31. K. Subrahmanya Sarma, C. Rambabu, G. Vishnu Priya, M.K. Raju, D. Parajuli, B.Khalid Mujasam, V. Ritesh, K. Rajesh, N. Murali, P.V. Lakshminarayana, Enhanced structural and magnetic properties of Al-Cr-substituted $SrFe_{12}O_{19}$ hexaferrite system, Appl. Phys. A, 2022, 128, 26. https://doi.org/10.1007/s00339-021-05164-7.
32. D.P. Sherstyuk, A.I. Kovalev, A.R. Zykova, V.E. Zhivulin, D.E. Zhivulin, D.A. Vinnik, Influence of the synthesis temperature on the structure and properties of highly Cr - substituted barium hexaferrite, J. Struct. Chem., 2025, 66, 176-187. https://doi.org/10.1134/S0022476625010160.
33. W. Wong-Ng, H.F. McMurdie, B. Paretzkin, M.A. Kuchinski, A.L. Dragoo, Standard X-Ray Diffraction Powder Patterns of Fourteen Ceramic Phases, Powder Diffr., 1988, 3, 246-254. https://doi.org/10.1017/S0885715600013579.
34. J. Qiu, Y. Wang, M. Gu, Effect of Cr substitution on microwave absorption of $BaFe_{12}O_{19}$, Mater. Lett., 2006, 60, 2728-2732. https://doi.org/10.1016/j.matlet.2006.01.079.
35. M. Awawdeh, I. Bsoul, S.H. Mahmood, Magnetic properties and Mössbauer spectroscopy on Ga, Al, and Cr substituted hexaferrites, J. Alloys Compd., 2014, 585, 465-473. https://doi.org/10.1016/j.jallcom.2013.09.174.
36. C.G. Koops, On the Dispersion of Resistivity and Dielectric Constant of Some Semiconductors at Audiofrequencies, Phys. Rev., 1951, 83, 121-124. https://doi.org/10.1103/physrev.83.121.
37. M.A.A.E. Darvish, Structural, magnetic and electrodynamic characteristics of functional magnetic materials based on substituted m-type hexaferrites, Ph.D. (Chem.) Dissertation, Moscow: National University of Science and Technology

"MISiS", 2021, (in Russian).
38. A. Thakur, R.R. Singh, P.B. Barman, Synthesis and characterizations of Nd3 doped $SrFe_{12}O_{19}$ nanoparticles, Mater. Chem. and Phys., 2013, 141, 562-569. http://doi.org/10.1016/j.matchemphys.2013.05.063.
39. K.W. Wagner, Dielectric relaxation in distributed dielectric layers, Ann. Phys., 1913, 40, 817.
40. J.C. Maxwell, Electricity and magnetism, Dover New York, 1954.
41. C. Kittel, Theory of the structure of ferromagnetic domains in films and small particles, Phys. Rev., 1946, 70, 965.
42. R.V. Mangalaraja, P. Manohar, F.D. Gnanam, M. Awano, Electrical and magnetic properties of $Ni_{0.8}Zn_{0.2}Fe_2O_4$/silica composite prepared by sol-gel method, J. Mater. Sci., 2004, 39, 2037-2042. https://doi.org/10.1023/B:JMSC.0000017766.07079.80.
43. B. Want, B.H. Bhat, B.Z. Ahmad, Effect of lanthanum substitution on dielectric relaxation, impedance response, conducting and magnetic properties of strontium hexaferrite, J. Alloys Compd., 2015, 627, 78-84. http://doi.org/10.1016/j.jallcom.2014.11.065 0925-8388.
44. P. Zhou, J. Zhang, H. Zhu, L. Wang, X. Wang, Z. Song, Q. Zhang, M. Yu, Z. Liu, T. Xu, W. Feng, X. Feng, Silica-Modified Ordered Mesoporous Carbon for Optimized Impedance-Matching Characteristic Enabling Lightweight and Effective Microwave Absorbers, ACS Appl. Mater. Interfaces., 2020, 12, 23252-23260. https://doi.org/10.1021/acsami.9b23287.
45. M.A. Darwish, A.V Trukhanov, O.S. Senatov, A.T. Morchenko, S.A. Saafan, K.A. Astapovich, S.V Trukhanov, E.L. Trukhanova, A.A. Pilyushkin, A.S.B. Sombra, D. Zhou, R.B. Jotania, C. Singh, Investigation of AC-Measurements of Epoxy/Ferrite Composites, Nanomater., 2020, 10, 492. https://doi.org/10.3390/nano10030492.